ENG.ASCE.0001.1

Low-Cycle Fatigue Behavior of Reinforcing Steel

By J. B. Mander,[1] F. D. Panthaki,[2] and A. Kasalanati[3]

Abstract: ASTM A615 grade 40 ordinary deformed-steel reinforcing bars with a specified minimum yield strength of 276 MPa (40 ksi) and ASTM A722 high-strength prestressing thread bars with a specified ultimate strength of 1,083 MPa (157 ksi) were experimentally evaluated for their low-cycle fatigue behavior under axial-strain–controlled reversed cyclic tests with strain amplitudes ranging from yield to 6%. All tests were performed on virgin (unmachined) specimens to closely simulate seismic behavior in structural concrete members. A methodology is suggested to identify incipient (first-cracking) failure of test specimens. The experimental data were evaluated with existing fatigue models, which related stress-strain quantities to the failure life. Additional energy-based fatigue models are proposed that relate various stress and/or strain quantities to the dissipated energy. The study demonstrates that the modulus of toughness and low-cycle fatigue life for both the low- and high-strength materials are similar. Based on fatigue considerations, it is concluded that existing design codes are overly restrictive in not permitting the use of high-strength thread bars in seismic-resisting elements.

Downloaded from ascelibrary.org by Dianna Roberts on 07/15/12. For personal use only.
No other uses without permission. Copyright (c) 2012. American Society of Civil Engineers. All rights reserved.

J. Mater. Civ. Eng. 1994.6:453-468.

INTRODUCTION

In a seismic event, the longitudinal reinforcing steel in reinforced or bonded prestressed structural concrete members may be expected to undergo large tension and compression strain reversals of typically one to five fully reversed equiamplitudes (Mander et al. 1992). Fracture of longitudinal reinforcing steel due to low-cycle fatigue is one of the prominent failure modes for flexural members with or without low levels of axial load. Such behavior is typical for bridge piers as well as the beams and columns in building frames where large cyclic-strain amplitudes up to 0.06 may be expected in medium- to high-seismic-risk zones. It is therefore important to understand the fatigue characteristics of reinforcing steels for seismic applications. Experimental fatigue test data for this very-low-cycle fatigue range do not seem to exist. This is because the vast majority of fatigue tests are generally conducted for mechanical engineering applications that mostly deal with medium- to high-cycle fatigue (10^3–10^7 cycles). For this class of testing, machined specimens are commonly used and strain amplitudes rarely exceed 0.01.

According to current practice, specimens for low-cycle fatigue tests are usually machined to form a smooth reduced section having either a parallel or hour-glass–shaped profile over the central test length [ASTM E606-80 ("Standard Recommended" 1987)]. In the process of manufacturing steel reinforcement for concrete structures, the reinforcing bars have deformations formed as part of the rolling process, and thus the material near the bar surface tends to become case-hardened. If this outer hardened material

[1]Asst. Prof., Dept. of Civ. Engrg., State Univ. of New York, 212 Ketter Hall, Box 604300, Buffalo, NY 14260.

[2]Former Grad. Res. Asst., Dept. of Civ. Engrg., State Univ. of New York, Buffalo, NY.

[3]Grad. Res. Asst., Dept. of Civ. Engrg., State Univ. of New York, Buffalo, NY.

Note. Discussion open until April 1, 1995. To extend the closing date one month, a written request must be filed with the ASCE Manager of Journals. The manuscript for this paper was submitted for review and possible publication on August 12, 1993. This paper is part of the ***Journal of Materials in Civil Engineering***, Vol. 6, No. 4, November, 1994. ©ASCE, ISSN 0899-1561/94/0004-0453/$2.00 + $.25 per page. Paper No. 6782.

J. Mater. Civ. Eng. 1994.6:453-468.
Downloaded from ascelibrary.org by Dianna Roberts on 07/15/12. For personal use only.
No other uses without permission. Copyright (c) 2012. American Society of Civil Engineers. All rights reserved.

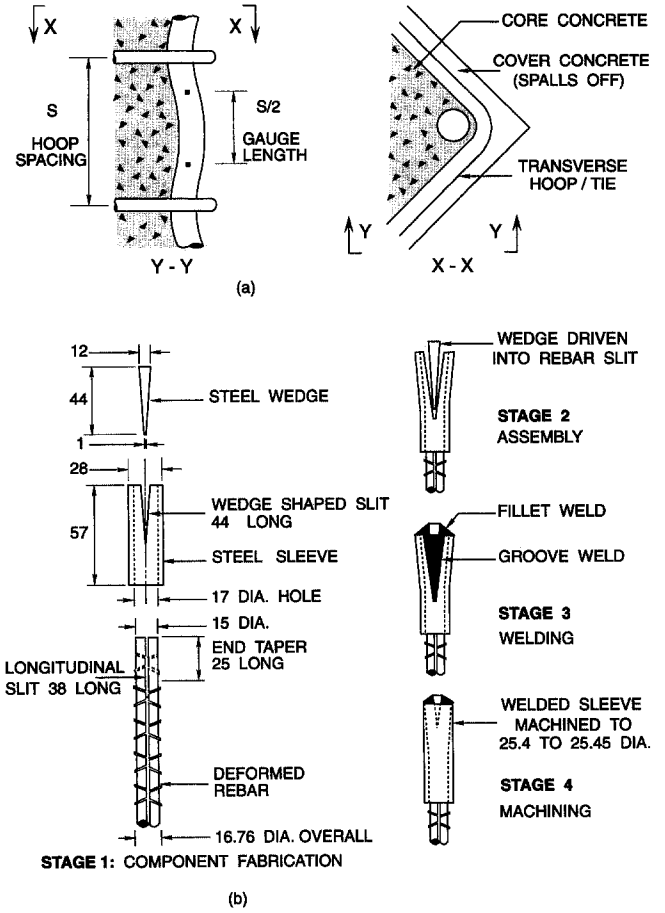

FIG. 1. Physical Modeling of Reinforcing Steel Behavior: (*a*) In Situ Conditions of Reinforcing Bar; and (*b*) Specimen Fabrication Procedure

is removed by machining off the deformations to obtain a smooth round specimen, the results obtained may not accurately reflect the actual behavior of the bar. It was thus felt important to leave the original cross section of the deformed reinforcing bar unaltered during testing and to directly capture the inelastic buckling that occurs in the compression region of a structural concrete element as shown in Fig. 1(*a*).

Two types of bars can potentially be used as longitudinal reinforcement in structural concrete members. Traditionally deformed mild-steel bars ranging from grade 40 to 60 (275–420 MPa) have been commonly used in reinforced concrete elements. More recently, there has been an interest in using high-strength steel and concrete materials for construction. Such materials are not encouraged by seismic codes because of their perceived brittleness. Thus, high-strength alloy-steel bars, usually used in prestressed concrete construction but potentially useful in seismic design, and conventional deformed reinforcing bars were investigated in this test program.

The objective of the research described here was to simulate constant-

amplitude cyclic fatigue conditions, with an emphasis on low cycle fatigue for longitudinal reinforcement under a representative range of seismic strain amplitudes, and to evaluate the experimental data using existing fatigue models.

SPECIMEN PREPARATION

The first type of material used was ASTM A722 type II hot-rolled and proof-stressed alloy-steel thread bar ("Specification" 1987) having a specified minimum ultimate tensile strength of 1,083 MPa. The surface deformations on this bar are in the form of continuous coarse threads rolled onto the entire length of the bar. The reason for selecting this particular thread bar over other types of high-strength steel reinforcement was to use couplers directly in gripping the virgin test specimen in the hydraulic grips of the testing machine.

For the high-strength thread bars, each test specimen consisted of 15.88-mm- (5/8-in.-) nominal-diameter (d_b) thread bar with the associated coupler 32-mm in diameter machined down to 25.4 mm with a 0.05-mm tolerance to meet the testing-machine grip-size requirements. The machined screw-on couplers were threaded onto each end of the specimen acting as end sleeves, which were by the test machine's hydraulic grips. This provided an excellent simulation of the in situ restraint provided by transverse reinforcement to prevent longitudinal bar buckling, as shown in Fig. 1(*a*).

The second type of material used was ASTM A615 grade 40 deformed billet-steel reinforcing bar ("Standard Specification" 1987) having a minimum specified yield strength of 276 MPa (coupon tensile tests are shown for both materials in Fig. 2, where specimens P1 and R13 represent the high-strength thread bar and mild-steel deformed bars, respectively). In contrast to the threadlike deformations of the high-strength bars, the surface deformations on the deformed bar were in the form of two diametrically opposed longitudinal ribs with connecting ribs inclined to the bar axis running between them over the surface of each half of the bar, as shown in Fig. 1(*b*). The absence of a regular threadlike pattern of deformations posed a significant challenge for the preparation of the end sleeves for the de-

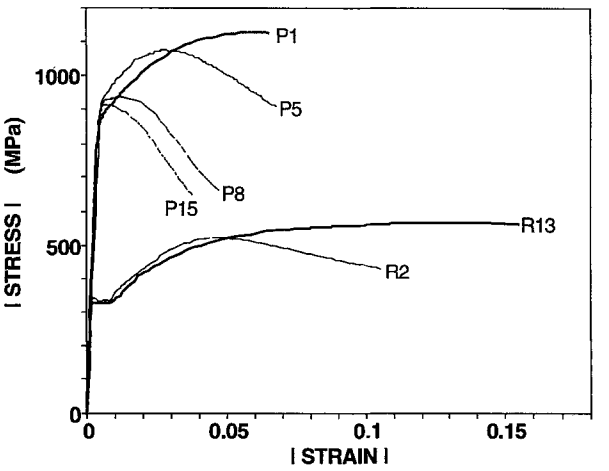

FIG. 2. Stress-Strain Results for Monotonic Tests

J. Mater. Civ. Eng. 1994.6:453-468.
Downloaded from ascelibrary.org by Dianna Roberts on 07/15/12. For personal use only.
No other uses without permission. Copyright (c) 2012. American Society of Civil Engineers. All rights reserved.

formed reinforcing bars. The various stages in reinforcing-bar specimen preparation are shown in Fig. 1(*b*).

Stage 1 shows the various components required for the fabrication of each end sleeve of the specimens. A 17-mm-diameter longitudinal hole was drilled in each piece of 28-mm-diameter plain round bar. This hole was marginally larger than the outer diameter of the bar measured over the surface deformations and was necessary for as tight a fit as possible of the specimen in the sleeve. The longitudinal saw cut made along the sleeve diameter was designed to facilitate outward splaying of the cut halves of the sleeve when the wedge was driven into the slit of the bar. In Stage 2, the specimen was slipped into the end sleeve and the steel wedge driven into the slit at the bar end, forcing the bar surface to crush against the inside of the sleeve, thereby causing the sleeve to splay out. The splayed-out end of the bar in the sleeve served as an excellent mechanical grip preventing the bar from being pulled out in tension. For preventing the bar from being pushed through in compression, some fillet welding was done at the bar end together with groove welding along the slits on each side of the sleeve. This is shown as stage 3 of the process in Fig. 1(*b*). Extreme care was taken to protect the test-gauge length of the bar from the high-temperature effects of the welding process by rapidly quenching the fresh welds in cold water. Finally, in stage 4, the welded end sleeves were machined to a uniform bar diameter of 25.4 mm to fit into the hydraulic grip collars. Subsequent testing showed that the anchorages for the thread bar and deformed bars were, respectively, capable of sustaining 100% and 97.5% of the ultimate tensile strength measured in coupon tests.

EXPERIMENTAL PROGRAM AND TESTING PROCEDURES

Tests were performed using an axial torsional machine, model 809.40, from MTS Systems Corp., Minneapolis, with hydraulic collet grips having a 250-kN axial tensile force capacity and a 60-MPa maximum clamping pressure. This automated electrohydraulic servocontrolled test system was capable of performing constant or variable amplitude load, strain, or deformation controlled tests. The lateral support spacing of six bar diameters was chosen for all the cyclic tests for both types of steel based on previous work by Mander et al. (1984), who tested numerous New Zealand–manufactured 275-MPa mild-steel reinforcing bars under uniaxial compression using this support spacing.

Axial strain was measured over the central three bar diameters (47.63-mm gauge length), of the specimen with a custom-built extensometer. This gauge length corresponded to mounting the transducer at the expected inflection points of a buckled specimen deformed in double curvature, thus giving the average strain for the specimen over its clear length. The test setup represents the center-to-center hoop spacing in a prototype concrete structure as shown in Fig. 1(*a*). A 12-mm stroke-conductive plastic linear-motion potentiometer mounted on the aluminum extensometer frame was used to measure the specimen displacement over the central half of the specimen. This extensometer arrangement permitted a total strain range of 0.13 to be measured with a resolution accuracy of ±15 microstrain. The tests were controlled externally by the extensometer with a sinusoidal wave form. Frequencies (f) ranged from 0.025 to 0.15 Hz, resulting in an average (peak-to-peak) strain rate of 0.005/s for most tests.

The task of defining an appropriate fatigue-failure criterion is a difficult one because past investigators have not been able to arrive at a consensus.

J. Mater. Civ. Eng. 1994.6:453-468.
Downloaded from ascelibrary.org by Dianna Roberts on 07/15/12. For personal use only.
No other uses without permission. Copyright (c) 2012. American Society of Civil Engineers. All rights reserved.

ENG.ASCE.0001.5

J. Mater. Civ. Eng. 1994.6:453-468.
Downloaded from ascelibrary.org by Dianna Roberts on 07/15/12. For personal use only.
No other uses without permission. Copyright (c) 2012. American Society of Civil Engineers. All rights reserved.

This is attributed to variations in the mode of test control (i.e., load or strain), number of cycles (high- versus low-cycle fatigue), the nature of test specimens and conditions, techniques for observation of crack growth, and final application of the test results. Many commonly used failure criteria are mentioned in the literature (Rao et al. 1985). For this study, incipient failure was defined as initiation of a fatigue crack in the test specimen. A detailed discussion of the failure condition in context of the test results follows.

Constant-amplitude low-cycle fatigue tests were categorized into two classes according to the strain ratio defined as $R = \varepsilon_{min}/\varepsilon_{max}$, where ε_{min} and ε_{max} are the largest compressive and tensile strains, respectively, with a sign convention of tension-positive. The completely reversed or equiamplitude tests ($R = 1$), which formed the vast majority of the cyclic tests, simulates typical strain histories of longitudinal reinforcement in columns under cyclic loading. Strain amplitudes up to 0.05 bars were used.

Partially reversed tests ($R \neq -1$) were performed with small compressive strains ($-0.004 < \varepsilon_{min} < 0$), approximately equal to yield strain, and significantly larger tensile strains. This class of cyclic loading represents the typical strain history for longitudinal reinforcement in reinforced or partially prestressed concrete beam or lightly loaded column elements subjected to seismic loading. The purpose for performing a few such tests was to verify Koh and Stephens' (1991) finding that, for total strain amplitudes $\varepsilon_a > 0.005$, testing with $R \neq -1$ did not cause a significant change in the fatigue life.

It was not possible to perform high-cycle fatigue tests on the specimens due to premature failure that occurred outside the central test region either within or adjacent to the coupler or grips. This limited the valid test range to 500 and 30,000 cycles for the reinforcing bars and high-strength thread bars, respectively.

EXPERIMENTAL RESULTS

Fig. 2 presents stress-strain curves for the monotonic tests. Their characteristic stress-strain control parameters for both material types are listed in Table 1. The test specimens are designated here with a prefix "P" for high-strength prestressing thread bar and a prefix "R" for deformed reinforcing bar, followed by a specimen number indicating the testing sequence. The stress convention used is tension-positive.

To determine the effects of the ratio of lateral support spacing to bar

TABLE 1. Monotonic Stress-Strain Parameters

Specimen (1)	Strain rate[a] (s^{-1}) (2)	s/d_b (3)	f_y (MPa) (4)	E_s (MPa) (5)	E_{sh} (MPa) (6)	ε_{sh} (7)	f_{su} (MPa) (8)	ε_{su} (9)	ε_{sf} (10)
P1	+0.005	6	869	221,300	11,030	0.0039	1,130	0.063	0.092
P5	−0.005	6	−917	220,600	12,130	−0.0041	−1,076	−0.028	—
P8	−0.005	8	−915	219,000	4,380	−0.0042	−936	−0.012	—
P15	−0.0005	9	−908	234,000	1,170	−0.0039	−914	−0.007	—
R13	—	9.6	331	215,100	8,274	0.0091	565	0.144	0.17
R2	−0.0002	6	−338	213,700	8,619	−0.0080	−531	−0.045	—

[a]Positive and negative strain rates are for tension and compression tests, respectively.

ENG.ASCE.0001.6

J. Mater. Civ. Eng. 1994.6:453-468.
Downloaded from ascelibrary.org by Dianna Roberts on 07/15/12. For personal use only.
No other uses without permission. Copyright (c) 2012. American Society of Civil Engineers. All rights reserved.

diameter (s/d_b) on the inelastic buckling properties of the steel, compressive tests were done for s/d_b ratios of 6, 8, and 9. For the specimen with smaller support spacing ($s = 6d_b$), the form of the compression stress-strain curve up to ultimate stress was similar to that of the tensile curve, except that the ultimate stress in compression was reached at a much lower strain than that for tension. After reaching the peak stress, the stress reduced gradually as the buckled profile increased with strain. At -0.065 strain, the stress was approximately equal to the yield stress. An increase in the support spacing ($s > 6d_b$) caused a decrease in the ultimate stress f_{su}^- and ultimate strain ε_{su}^- accompanied by substantial bar buckling and subsequent stress loss. Mander et al. (1988a) have shown experimentally that structural concrete columns with a high level of confinement may develop very high compressive strains exceeding 0.06 in the concrete. It is important to note that at such high strains, the longitudinal steel should be able to sustain the yield stress level to prevent premature column failure. Design codes require that center-to-center spacing between transverse reinforcement should not exceed eight [ACI 318 ("Building" 1989)] or six [NZS3101 ("The Design" 1982)] longitudinal bar diameters. Fig. 2 clearly shows that the NZS3101 requirement is satisfactory as the yield stress can be maintained up to a strain of 0.065, whereas for $s \geq 8d_b$, the yield stress drops off after strains as small as 0.015, which clearly indicates that the ACI 318 requirements are inadequate in this context for high-strength steel.

Results of the various low-cycle fatigue tests are listed in Table 2, with Figs. 3 and 4 presenting a selection of the stress-strain curves. Representative hysteresis loops for some small-amplitude tests are shown in Figs. 3(*a*), 3(*c*), and 3(*e*). Axial-strain–controlled, low-cycle fatigue testing causes cyclic softening in hot-rolled and proof-stressed prestressing thread bars, as shown in Figs. 3(*b*) and 3(*f*), and cyclic hardening in ordinary deformed reinforcing bars, in Fig. 3(*d*). These graphs plot the normalized stress at reversal (f_i/f_0) versus the number of cycles (i) for specimen numbers P2, P3, and R8, respectively. Here f_i is defined as the stress at maximum strain (i.e., stress at the point of reversal) for the ith cycle and f_0 the stress at first reversal. The cyclic hardening or softening continues until a saturation state is reached when f_i/f_0 remains at an almost constant level. This stabilized behavior is observed until a fatigue crack forms, after which the stress at reversal in tension starts dropping rapidly with further cycling until complete fracture (separation) occurs. The instant when the normalized tensile stress at reversal starts dropping below the normalized saturation stress level was selected as the onset of failure, and the number of cycles to failure was defined as N_f. Thus, for the small-strain-amplitude tests ($\varepsilon_a < 0.02$) resulting in a large number of cycles, the value of N_f was determined using the methodology as described.

An interesting characteristic of the small-amplitude test stress-strain graphs after crack initiation is cusp formation, which corresponds to the change in shape of the stress-strain hysteresis loop indicated by a well-developed inflexion point in the peak compressive region of the loop. Figs. 3(*a*), 3(*c*), and 3(*e*) show that the cusp becomes more pronounced with further cycling. Furthermore, the rate of fall of the peak compressive stress at reversal (f_i/f_0) in Figs. 3(*b*), 3(*d*), and 3(*f*) after crack initiation for any cycle after N_f is decidedly lower than that in tension. This phenomenon can be attributed to fracture-crack propagation.

Fig. 4 shows stress-strain graphs for some of the large amplitude tests. Figs. 4(*a*)–4(*d*) show equiamplitude ($R = -1$) test results for thread bar

ENG.ASCE.0001.7

J. Mater. Civ. Eng. 1994.6:453-468.
Downloaded from ascelibrary.org by Dianna Roberts on 07/15/12. For personal use only.
No other uses without permission. Copyright (c) 2012. American Society of Civil Engineers. All rights reserved.

TABLE 2. Low-Cycle Fatigue Test Results

ε_a (1)	Specimen (2)	R (3)	f (Hz) (4)	ε_{ap} (5)	N_f (6)	ΔW_p (MPa) (7)	W_{jT} (MPa) (8)
0.092	P1	0	—	0.0879	0.25	—	92[b]
0.062	P19	−0.266	—	0.0549	0.75	181.5	136
0.05	P18	−1	0.025	0.0412	2.1	122.5	253
0.045	P10	−1	0.028	0.0379	2.2	114.0	261
0.04	P13	−1	0.031	0.0333	3.0	91.1	285
0.035	P17	−0.04	0.042	0.0280	5.4	70.2	418
0.035	P12	−1	0.036	0.0283	6.1	76.3	468
0.03	P4	−1	0.1[a]	0.0246	7.2	71.5	525
0.025	P7	−1	0.05	0.0205	9.2	56.3	529
0.02375	P16	−0.0085	0.063	0.0190	10.4	48.7	535
0.02	P14	−1	0.063	0.0148	18	42.5	799
0.0175	P9	−1	0.071	0.0131	21	34.0	725
0.015	P6	−1	0.083	0.0107	32	26.6	876
0.0125	P11	−1	0.1	0.0089	63	21.6	1,445
0.01	P3	−0.25	0.1	0.0065	103	14.9	1,531
0.01	P2	−1	0.1[a]	0.0065	103	15.2	1,620
0.0084	P21	−1	0.125	—	207	9.75	2,317
0.00635	P22	−1	0.25	—	605	6.06	3,765
0.0054	P23	−1	0.25	—	810	4.28	3,613
0.003	P24	−1	0.5	—	4,450	1.21	5,378
0.0026	P25	−1	0.5	—	9,300	0.79	7,446
0.0025	P26	−1	0.5	—	12,500	0.82	10,343
0.002	P27	−1	1.0	—	26,500	—	—
0.17	R13	0	—	0.169	0.25	—	88[b]
0.04	R12	−3	0.031	0.037	2.5	59.2	168
0.03	R1	−1	0.042	0.027	4.1	44.6	175
0.025	R9[c]	−1	0.05	0.022	5.6	35.8	199
0.02	R5	−1	0.063	0.018	9.2	27.4	252
0.0175	R11[c]	−1	0.072	0.016	13	23.1	301
0.015	R7	−1	0.083	0.013	21	19.2	403
0.0134	R21	−1	0.0933	0.0117	25	16.3	423
0.0125	R10[c]	−1	0.1	0.0110	23	15.2	350
0.01	R4	−1	0.12	0.0083	49	11.0	542
0.008	R8	−1	0.15	0.0065	148	8.3	1,227

[a]Different strain rate from the standard peak-to-peak average of 0.005/s.
[b]Modulus of toughness for monotonic test.
[c]Initial strain direction was in compression.

and reinforcing bar, respectively. Figs. 4(*e*) and 4(*f*), respectively, show unequal-amplitude test results for thread bar ($R = -0.04$) and reinforcing bar ($R = -3$). For larger strain amplitudes ($\varepsilon_a > 0.02$), a modification to the procedure for selecting N_f was necessitated by the fact that at these large amplitudes, the stress at reversal (f_i) decreased continuously. Thus, there was no well-defined saturation level from which the fall in f_i could be indentified to locate N_f at crack initiation. The onset of cracking was indicated both visually and by a backward shift of the strain corresponding

J. Mater. Civ. Eng. 1994.6:453-468.
Downloaded from ascelibrary.org by Dianna Roberts on 07/15/12. For personal use only.
No other uses without permission. Copyright (c) 2012. American Society of Civil Engineers. All rights reserved.

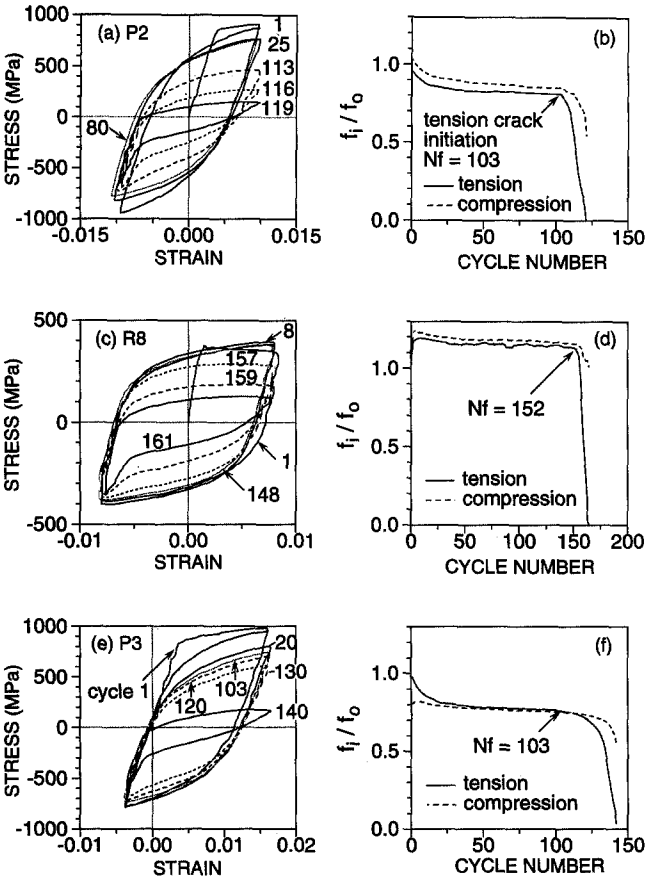

FIG. 3. Cyclic Stress-Strain Results for (*a*) Hysteresis Loop, Specimen P2; (*b*) Fatigue Testing, Specimen P2; (c) Hysteresis Loop, Specimen R8; (d) Fatigue Testing, Specimen R8; (*e*) Hysteresis Loop, Specimen P3; and (*f*) Fatigue Testing, Specimen P3

to the peak tensile stress when the peak stress occurred at a lower strain value than the strain amplitude and decreased as it approached the maximum strain amplitude. This instant, indicated by an "x" on the stress-strain graphs, was closely followed by complete failure of the specimen.

The total energy dissipated until specimen failure W_{fT} was calculated by numerically integrating of the area enclosed within the hysteresis loops for the entire test history. Values for cyclic hysteresis energy ΔW_p, which is the area of the loop at half-life (i.e., when $N_i = N_f/2$), are also reported along with W_{fT} values in Table 1. The table also includes, for completeness, the results for the monotonic tension test where the final fracture strain ε_{sf} was selected as the value for the strain amplitude ε_a, and $N_f = 0.25$. Here, the total energy dissipated is equivalent to the modulus of toughness, and is approximately the same for both types of steel. This result is consistent with the findings of Mander et al. (1988b) for other types of reinforcing steel.

J. Mater. Civ. Eng. 1994.6:453-468.
Downloaded from ascelibrary.org by Dianna Roberts on 07/15/12. For personal use only.
No other uses without permission. Copyright (c) 2012. American Society of Civil Engineers. All rights reserved.

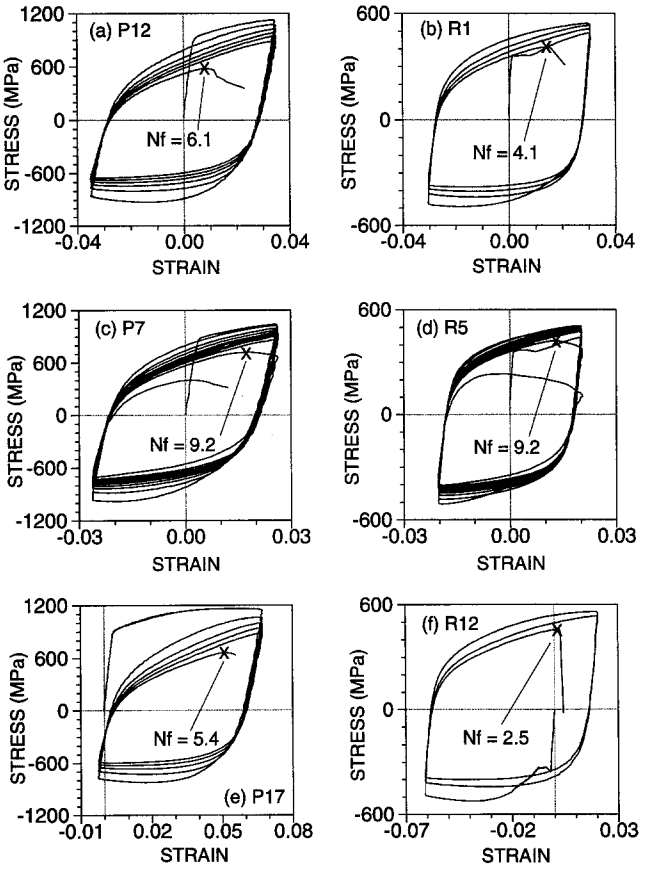

FIG. 4. Cyclic Stress-Strain Results for (*a*) Specimen P10, Equiamplitude, (*b*) Specimen R5, Equiamplitude; (*c*) Specimen P17, Equiamplitude; (*d*) Specimen R12, Equiamplitude; (*e*) Specimen P12, Unequal Amplitude; and (*f*) Specimen R1, Unequal Amplitude

MEAN STRESS AND STRAIN EFFECTS

Mean stress effects come into play for longer fatigue lives that have a predominantly elastic strain component. For cases that have low strain amplitudes (<0.005), the fatigue life may increase or decrease depending on the sign of the mean stress being compressive or tensile (Koh and Stephens 1991). At higher strain amplitudes, where plastic strains are significant, mean stress relaxation occurs, which tends to reduce any mechanically or thermally induced mean stresses toward zero or a very small value such that it has no perceptible effect on the fatigue life. Thus, for the range of strain amplitudes used for the study of low-cycle fatigue (1–6%), mean stress effects are negligible. This was confirmed by observing the results of the partially reversed tests, all of which had nonzero mean strains. Figs. 5 and 6 show that for all R values other than -1, the data points fit very well with the general trend of the other completely reversed ($R = -1$) tests. For medium- to high-cycle fatigue tests, these effects were not investigated.

ENG.ASCE.0001.10

J. Mater. Civ. Eng. 1994.6:453-468.
Downloaded from ascelibrary.org by Dianna Roberts on 07/15/12. For personal use only.
No other uses without permission. Copyright (c) 2012. American Society of Civil Engineers. All rights reserved.

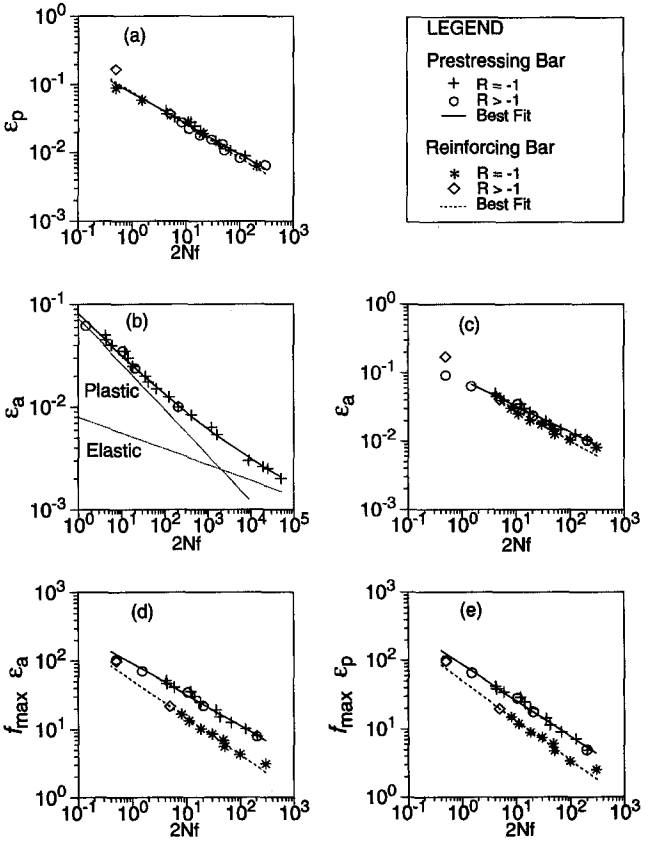

FIG. 5. Experimental Data Fit to Existing Fatigue Models: (*a*) Coffin—Manson Model for Plastic Strain; (*b*) Coffin—Manson Model for Total Strain; (*c*) Koh—Stephens Model; (*d*) Modified SWT Model; and (*e*) Lorenzo—Laird Model

APPLICATION OF EXISTING FATIGUE-LIFE MODELS TO RESULTS

In this section, test results are analyzed by considering the applicability of several various predictive strain (and stress) fatigue-life models. As the utility of these existing fatigue models is somewhat limited in application, a more applicable energy-based approach is developed. The following discussion describes the various fatigue models found in literature. Each model can be plotted in a logarithmic form with the values of model coefficients and exponents being obtained from a linearized (log-log) least-squares regression analysis. The results are reported along with the value of the square of the correlation coefficient r in Table 3. N_f and $2N_f$ mean the number of cycles and reversals, respectively.

The initial Coffin—Manson equation (Coffin 1954; Manson 1953) related plastic-strain amplitude (ε_{ap}) with fatigue-life data as follows:

$$\varepsilon_{ap} = \frac{\Delta\varepsilon_p}{2} = \varepsilon_f'(2N_f)^c \tag{1}$$

The fit of this model to the experimental data is shown in Fig. 5(*a*). This

J. Mater. Civ. Eng. 1994.6:453-468.
Downloaded from ascelibrary.org by Dianna Roberts on 07/15/12. For personal use only.
No other uses without permission. Copyright (c) 2012. American Society of Civil Engineers. All rights reserved.

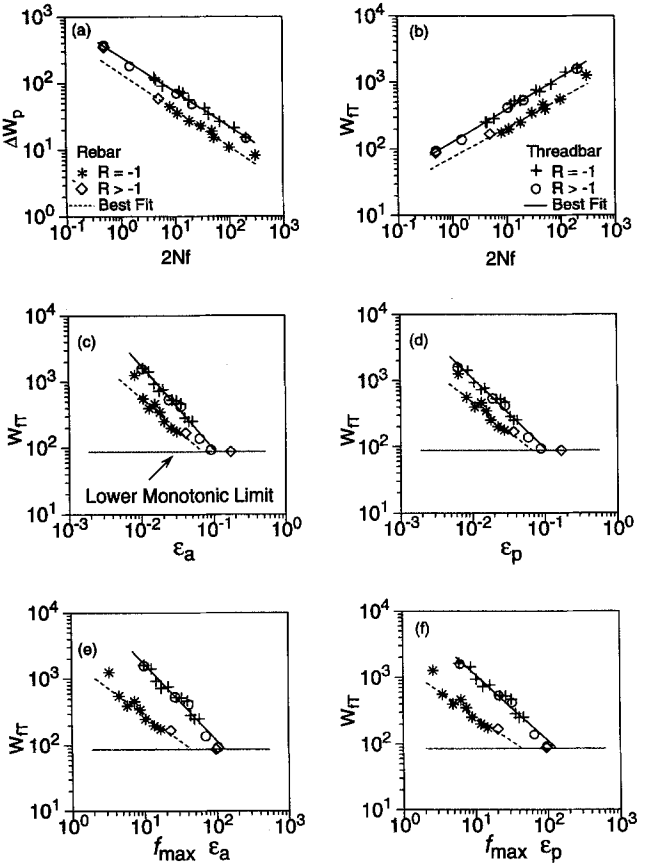

FIG. 6. Experimental Data Fit to: (*a*) Existing Energy-Fatigue Models of Tong et al. (1989) for Cyclic Energy; (*b*) Existing Energy-Fatigue Models of Tong et al. (1989) for Total Energy; (*c*) Proposed Energy-Based Models for Total Strain; (*d*) Proposed Energy-Based Models for Plastic Strain; (*e*) Proposed Energy-Based Models for Stress and Total Strain; and (*f*) Proposed Energy-Based Models for Stress- and Plastic-Strain Amplitude

and subsequent graphs plot the results for both the high-alloy prestressing thread bars (curve P) and ordinary mild-steel deformed reinforcing bars (curve R). It is evident that a single curve could be developed to be universally applicable to all reinforcing steels such as

$$\varepsilon_{ap} = 0.08(2N_f)^{-0.5} \tag{2}$$

Instead of using plastic-strain amplitude, which can be somewhat difficult to define due to Bauschinger effects, one variant of the Coffin—Manson relationship used the total strain amplitude (ε_a), used by Koh and Stephens (1991) and is given by

$$\varepsilon_a = \frac{\Delta\varepsilon}{2} = M(2N_f)^m \tag{3}$$

ENG.ASCE.0001.12

J. Mater. Civ. Eng. 1994.6:453-468.
Downloaded from ascelibrary.org by Dianna Roberts on 07/15/12. For personal use only.
No other uses without permission. Copyright (c) 2012. American Society of Civil Engineers. All rights reserved.

TABLE 3. Results of Fatigue-Life Models

Model (1)	Equation number (2)	Bars (3)	Best fit (4)	r^2 (5)
Coffin—Manson	1	Prestressing	$\varepsilon_{ap} = 0.0749(2N_f)^{-0.451}$	0.990
Coffin—Manson	1	Reinforced	$\varepsilon_{ap} = 0.0777(2N_f)^{-0.486}$	0.984
Koh—Stephens	2	Prestressing	$\varepsilon_a = 0.0791(2N_f)^{-0.381}$	0.989
Koh—Stephens	3	Reinforced	$\varepsilon_a = 0.0795(2N_f)^{-0.448}$	0.985
Modified SWT	5	Prestressing	$f_{max}\varepsilon_a = 91.4(2N_f)^{-0.452}$	0.985
Modified SWT	5	Reinforced	$f_{max}\varepsilon_a = 51.6(2N_f)^{-0.541}$	0.991
Lorenzo—Laird	8	Prestressing	$f_{max}\varepsilon_{ap} = 86.7(2N_f)^{-0.522}$	0.986
Lorenzo—Laird	8	Reinforced	$f_{max}\varepsilon_{ap} = 50.6(2N_f)^{-0.581}$	0.988
TWX cyclic energy	10	Prestressing	$\Delta W_p = 252(2N_f)^{-0.523}$	0.993
TWX cyclic energy	10	Reinforced	$\Delta W_p = 142(2N_f)^{-0.550}$	0.868
TWX total energy	11	Prestressing	$W_{fT} = 126.2(2N_f)^{0.486}$	0.993
TWX total energy	11	Reinforced	$W_{fT} = 74.4(2N_f)^{0.439}$	0.968
Energy—Strain Amplitude	12*a*	Prestressing	$W_{fT} = 5.09(\varepsilon_a)^{-1.268}$	0.973
Energy—Strain Amplitude	12*a*	Reinforced	$W_{fT} = 6.72(\varepsilon_a)^{-0.961}$	0.914
Energy—Plastic-Strain Amplitude	12*b*	Prestressing	$W_{fT} = 7.93(\varepsilon_{ap})^{-1.070}$	0.974
Energy—Plastic-Strain Amplitude	12*b*	Reinforced	$W_{fT} = 8.00(\varepsilon_{ap})^{-0.884}$	0.911
Energy—Stress × Amplitude	12*c*	Prestressing	$W_{fT} = 24{,}126(f_{max}\varepsilon_a)^{-1.16}$	0.960
Energy—Stress × Amplitude	12*c*	Reinforced	$W_{fT} = 1{,}840(f_{max}\varepsilon_a)^{-0.80}$	0.922
Energy—Stress × Plastic Amplitude	12*d*	Prestressing	$W_{fT} = 10{,}782(f_{max}\varepsilon_a)^{-0.991}$	0.963
Energy—Stress × Plastic Amplitude	12*d*	Reinforced	$W_{fT} = 1{,}456(f_{max}\varepsilon_a)^{-0.745}$	0.918

The results for the present tests are plotted in Fig. 5(*c*), from which the scatter of data points is minimal and all the points fall close to the least-squares line.

The fatigue life of a material subjected to a given strain range could be estimated by superposition of the elastic- and plastic-strain components, given by another variation of Coffin-Manson relationship as:

$$\varepsilon_a = \frac{\Delta\varepsilon}{2} = \frac{\sigma_f'}{E}(2N_f)^b + \varepsilon_f'(2N_f)^c \tag{4}$$

The total strain–fatigue-life curve approaches the plastic-strain life curve at large strain amplitudes and approaches the elastic-strain life curve at low strain amplitudes. The fit of this model to the experimental data is shown in Fig. 5(*b*). In this plot, the values of material fatigue constants corresponding to elastic-strain component were $\sigma_f'/E = 0.008$ and $b = -0.14$, and may vary up to 10% because of lack of data in the range $N_f > 10^6$.

It is also of interest to observe the relevance of test data to a couple of mean stress models. One popular model that accounts for the effects of

ENG.ASCE.0001.13

mean stress was proposed by Smith et al. (1970) (referred to as the SWT model). The original form of the stress-strain function was given by

$$\sqrt{f_{\max}\varepsilon_a E_s} = f(2N_f) \tag{5}$$

where $f_{\max}$ = maximum tensile stress at the half-life of each test. The original function in (5) was further generalized into a bilinear equation to account for the entire low- and high-cycle fatigue range:

$$f_{\max}\varepsilon_a = A_1(N_f)^{a_1} + A_2(N_f)^{a_2} \tag{6}$$

Subsequently, (6) was simplified for low-cycle fatigue modeling of high-strength pressure-vessel steel (monotonic yield strength of 1,170 MPa) by Koh and Stephens (1991) in the general form

$$f_{\max}\varepsilon_a = C(2N_f)^{\gamma} \tag{7}$$

It is evident from the results presented in Fig. 5(*d*) that this modified SWT model in (6) fits the experimental data for both bar types quite well. The value of the coefficient C is dependent on the strength of the material. It appears that a common value of $\gamma = -0.5$ could be adopted for both reinforcing steel types, with the model conforming to the original SWT form in (5).

Fig. 5(*e*) presents the results for a plastic strain version of the modified SWT function proposed by Lorenzo and Laird (1984). Their relationship is given by

$$f_{\max}\varepsilon_{ap} = L(2N_f)^{l} \tag{8}$$

ENERGY-BASED MODELING

From (6) and (8), it is evident that the product $f_{\max}\varepsilon_a$ or $f_{\max}\varepsilon_{ap}$ implicitly gives a measure of the work done for one cycle of loading. For example, Sugiura et al. (1991) proposed the following model for structural metals under multiaxial stresses:

$$N_f = C_1(f_{\max})^{c_2}(\Delta W_p)^{c_3} \tag{9}$$

where c_1, c_2, and c_3 = material constants, $c_1 = 2.55 \times 10^8$, $c_2 = -1.67$, and $c_3 = 0.987$ for 1% Cr-Mo-V steel. Tong et al. (1989) also used an energy-life concept to relate the hysteretic energy ΔW_p for one cycle at half-life to fatigue life by the relation

$$\Delta W_p = W_f'(2N_f)^{\beta} \tag{10}$$

where W_f' and β = material constants. The results plotted in Fig. 6(*a*) show that this model works well for both the mild and high strength of reinforcing steels.

It is evident that by multiplying both sides of (10) by N_f the total energy dissipated can be related to the failure life. Previous studies by Tong et al. (1989) and Lefebvre and Ellyin (1984) have indicated that for a fully reversed constant-strain–controlled test, there is negligible variation in the cyclic hysteresis energy with the number of cycles during fatigue life, and its value at the cycle at half-life can be used as a characteristic of the entire test. Tong et al. (1989) modified their previous solution by multiplying both sides of (10) by N_f to give total energy absorption capacity as follows.

$$W_{fT} = W_{fT}'(2N_f)^{1+\beta} \tag{11}$$

J. Mater. Civ. Eng. 1994.6:453-468.
Downloaded from ascelibrary.org by Dianna Roberts on 07/15/12. For personal use only.
No other uses without permission. Copyright (c) 2012. American Society of Civil Engineers. All rights reserved.

ENG.ASCE.0001.14

where W'_{fT} = a material constant. Fig. 6(*b*) presents the results of this model and shows good agreement with (11). This total energy life model provides the basis for developing a suite of energy-based fatigue models described in the following section.

Here, it is proposed to combine the form of the strain-life fatigue models of (1)–(7) with (11). By eliminating the number of reversals ($2N_f$), the total energy dissipated can be directly related to the strain amplitude and maximum stress. The following forms of energy-based fatigue models are proposed:

$$W_{fT} = W_a(\varepsilon_a)^p \tag{12a}$$

$$W_{fT} = W_{ap}(\varepsilon_{ap})^q \tag{12b}$$

$$W_{fT} = W_{fa}(f_{\max}\varepsilon_a)^r \tag{12c}$$

$$W_{fT} = W_{fap}(f_{\max}\varepsilon_{ap})^s \tag{12d}$$

where W_a, W_{ap}, W_{fap}, W_{fp}, p, q, r, and s = material constants. Here, the value of $f_{\max}$ has been modified as the magnitude of the maximum stress (tension or compression) in the entire strain history for the original definition of maximum tensile stress at half-life to cater for cumulative damage modeling applications for a random history. The application of each model in (12*a*)–(12*d*) to the test data is illustrated in Fig. 6, with values of the best-fit equations together with their respective correlation coefficients reported in Table 2. In all cases, there is satisfactory agreement between the model and the test results. The total energy dissipated has a lower-bound cut-off value, which is the value for the monotonic tension test as indicated in the plots.

In the preceding regression analyses, except for (4) only the data in the true low-cycle fatigue strain range were used, i.e., $0.009 < \varepsilon_a < 0.07$. Data outside this range either were in the transition region to high-cycle fatigue or represented monotonic tests.

SUMMARY AND CONCLUSIONS

The testing of unmachined steel in reversed cyclic loading required special gripping techniques to be applied to enable high (near-ultimate) stresses to be attained in both tension and compression. Thread bars can be easily tested by machining down the couplers to meet the test-machine requirements. However, the testing of deformed reinforcing bars in their virgin state requires the attachment of special end grips onto the bar itself. As part of this study, an effective test methodology was developed that enabled low-cycle fatigue tests to be performed on deformed reinforcing bars permitting 100% and 97% of the respective ultimate compression and tension stresses to be attained.

If a lateral support spacing of six longitudinal bar diameters or less is provided ($s \leq 6d_b$), then a stress greater than yield can be sustained over the entire compression range expected in well confined structural concrete members. Thus, no design limits need to be placed on the allowable strain ranges. If the spacing is greater than six bar diameters, then the compression strength can only be maintained over a limited range. This range decreases as the support spacing increases. If $s > 8d_b$, the yield strength will be attained but not sustained.

For high-strength bars under cyclic-strain reversals, the peak cycle stress

J. Mater. Civ. Eng. 1994.6:453-468.
Downloaded from ascelibrary.org by Dianna Roberts on 07/15/12. For personal use only.
No other uses without permission. Copyright (c) 2012. American Society of Civil Engineers. All rights reserved.

ENG.ASCE.0001.15

drops quickly in the first few cycles, i.e., softening occurs, whereas for reinforcing bars, cycling causes hardening over the first few cycles, after which the peak cycle stress decreases very gradually almost constant over a large number of cycles until incipient failure occurs at the onset of a fatigue crack. Cycling can still continue, but the crack propagates quickly with the peak stress dropping rapidly until fracture occurs.

For low-cycle fatigue tests on ordinary deformed reinforcing steel bar or high-strength prestressing-steel thread bar with large strain amplitudes (1–5%) typical of segments from longitudinal reinforcement histories under strong seismic excitations, mean stress and mean strain have negligible effect on low-cycle fatigue life.

The behavior of the test specimens considered in this study conform well to the commonly used strain-life models for low-cycle fatigue. The proposed energy-based fatigue models may also prove useful in seismic analysis.

For seismic design, conventional wisdom requires ductile detailing that maximizes the displacement/curvature ductility in the structural elements. In this study, the displacement ductility ($\varepsilon_{su}/\varepsilon_y$) of the high-strength steel thread bar is only 17% of the deformed mild-steel bar. It is therefore not surprising that seismic codes limit the yield strength of the reinforcing steel to grade 60 (f_y = 414 MPa). This study has demonstrated that in spite of a meager displacement ductility for high-strength steel, the modulus of toughness and the plastic-strain–life properties for both materials are similar. The energy dissipation capacity for a given strain amplitude is superior for high-strength alloy steel when compared to high-strength mild-steel reinforcement. It appears that code restrictions on the use of such steel are unwarranted.

J. Mater. Civ. Eng. 1994.6:453-468.
Downloaded from ascelibrary.org by Dianna Roberts on 07/15/12. For personal use only.
No other uses without permission. Copyright (c) 2012. American Society of Civil Engineers. All rights reserved.

ACKNOWLEDGMENTS

The writers would like to thank Dywidag Systems International, Lincoln Park, NJ for its generous donation of the high-strength thread bars and couplers. Financial support from the National Center for Earthquake Engineering Research at the State University of New York at Buffalo is gratefully acknowledged.

APPENDIX I. REFERENCES

"Building code requirements for reinforced concrete." (1989). *ACI 318*, Am. Concr. Inst., Detroit, Mich.

Coffin, L. F. Jr. (1954). "A study of the effects of cyclic thermal stresses on a ductile metal." *Trans.*, American Society of Mechanical Engineers, New York, N.Y., 76, 931–950.

"The design of concrete structures." (1982). *NZS 3101, Part 1 Code of Practice; Part 2 Comm.* Standards Association of New Zealand, Wellington, New Zealand.

Koh, S. K., and Stephens, R. I. (1991). "Mean stress effects on low cycle fatigue for a high strength steel." *Fatigue Fracture of Engrg. Mater. and Struct.*, 14(4), 413–428.

Lefebvre, D., and Ellyin, F. (1984). "Cyclic response and inelastic strain energy in low cycle fatigue." *Int. J. Fatigue*, 6(1), 9–15.

Lorenzo, F., and Laird, C. (1984). "A new approach to predicting fatigue life behavior under the action of mean stresses." *Mater. Sci. and Engrg.*, 62(2) 205–210.

Mander, J. B., Panthaki, F. D., and Chaudhary, M. T. (1992). "Evaluation of seismic venerability of highway bridges in the eastern United States." *Lifeline earthquake engineering in the central and eastern U.S.*, D. B. Ballantyne, ed., ASCE, New York, N.Y., Sept., 72–86.

Mander, J. B., Priestley, M. J. N., and Park, R. (1984). "Seismic design of bridge

ENG.ASCE.0001.16

piers." *Research Report 84-2*, Univ. of Canterbury, Christchurch, New Zealand, Feb.
Mander, J. B., Priestley, M. J. N., and Park, R. (1988a). "Observed stress-strain behavior of confined concrete." *J. Struct. Engrg.*, ASCE, 114(8), 1827–1849.
Mander, J. B., Priestley, M. J. N., and Park, R. (1988b). "Theoretical stress-strain model for confined concrete." *J. Struct. Engrg.*, ASCE, 114(8), 1804–1826.
Manson, S. S. (1953). "Behavior of materials under conditions of thermal stress." *Heat Transfer Symp.*, University of Michigan Engineering Research Institute, Ann Arbor, Mich., 9–75.
Rao, K. B. S., Valsan, M., Sandhya, R., Ray, S. K., Mannan, S. L., and Rodriguez, P. (1985). "On the failure condition in strain-controlled low cycle fatigue." *Int. J. Fatigue*, 7(3), 141–147.
Smith, K. N., Watson, P., and Topper, T. H. (1970). "A stress-strain function for the fatigue of metals." *J. Mater.*, 5(4), 767–778.
"Specification for uncoated high-strength steel bar for prestressing concrete." (1987). ASTM A 722-86, *Annual book of ASTM standards*, ASTM, Philadelphia, Pa., 1.04, 668–672.
"Standard recommended practice for constant amplitude low-cycle fatigue testing." (1987). ASTM E 606-80, *Annual book of ASTM standards*, ASTM, Philadelphia, Pa., 3.01, 841–853.
"Standard specification for deformed and plain billet-steel bars for concrete reinforcement." (1987). ASTM A 615-86, *Annual book of ASTM standards*, ASTM, Philadelphia, Pa., 1.04, 510–514.
Sugiura, K., Chang, K. C., and Lee, G. C. (1991). "Evaluation of low-cycle fatigue of structural metals." *J. Engrg. Mech.*, ASCE, 117(10), 2373–2383.
Tong, X., Wang, D., and Xu, H. (1989). "Investigation of cyclic hysteresis energy in fatigue failure process." *Int. J. Fatigue*, 11(5), 353–359.

APPENDIX II. NOTATION

The following symbols are used in this paper:

d_b = bar diameter;
f = testing frequency;
f_m = mean stress = $(f_{max} + f_{min})/2$;
f_{max} = maximum (tension) stress;
f_{min} = minimum (compression) stress;
f_{su} = ultimate stress (monotonic);
N_f = cycles to failure;
R = strain ratio = $\varepsilon_{min}/\varepsilon_{max}$;
r^2 = square of correlation coefficient;
s = lateral support spacing;
W_{fT} = total energy dissipated to incipient failure;
ΔW_p = energy dissipated in one cycle;
$\Delta\varepsilon$ = total strain range = $\varepsilon_{max} - \varepsilon_{min}$;
$\Delta\varepsilon_p$ = total plastic-strain range;
ε_a = strain amplitude = $\Delta\varepsilon/2$;
ε_{ap} = plastic strain amplitude = $\Delta\varepsilon_p/2$;
ε_m = mean strain = $(\varepsilon_{max} + \varepsilon_{min})/2$;
ε_{max} = maximum (tension) strain;
ε_{min} = minimum (compression) strain; and
ε_{su} = strain at ultimate stress.

J. Mater. Civ. Eng. 1994.6:453-468.
Downloaded from ascelibrary.org by Dianna Roberts on 07/15/12. For personal use only.
No other uses without permission. Copyright (c) 2012. American Society of Civil Engineers. All rights reserved.